

Research Article

Antibody density on bacteria regulates C1q recruitment by monoclonal IgG but not IgM

Nathan Aymerich¹, Luca J. Schlotheuber², Olivia T. M. Bucheli², Kevin Portmann², Jean Baudry¹ and Klaus Eyer^{2,3} 

¹ Laboratoire Colloïdes et Matériaux Divisés (LCMD), ESPCI Paris, PSL Research University, CNRS UMR8231 Chimie Biologie Innovation, Paris, France

² Laboratory for Functional Immune Repertoire Analysis, Institute of Pharmaceutical Sciences, Department of Chemistry and Applied Biosciences, ETH Zürich, Zürich, Switzerland

³ Department of Biomedicine, Aarhus University, Aarhus, Denmark

Antibodies that trigger the complement system play a pivotal role in the immune defense against pathogenic bacteria and offer potential therapeutic avenues for combating antibiotic-resistant bacterial infections, a rising global concern. To gain a deeper understanding of the key parameters regulating complement activation by monoclonal antibodies, we developed a novel bioassay for quantifying classical complement activation at the monoclonal antibody level, and employed this assay to characterize rare complement-activating antibacterial antibodies on the single-antibody level in postimmunization murine antibody repertoires. We characterized monoclonal antibodies from various antibody isotypes against specific pathogenic bacteria (*Bordetella pertussis* and *Neisseria meningitidis*) to broaden the scope of our findings. We demonstrated activation of the classical pathway by individual IgM- and IgG-secreting cells, that is, monoclonal IgM and IgG2a/2b/3 subclasses. Additionally, we could observe different epitope density requirements for efficient C1q binding depending on antibody isotype, which is in agreement with previously proposed molecular mechanisms. In short, we found that antibody density most crucially regulated C1q recruitment by monoclonal IgG isotypes, but not IgM isotypes. This study provides additional insights into important parameters for classical complement initiation by monoclonal antibodies, a knowledge that might inform antibody screening and vaccination efforts.

Keywords: B cells · Bacterial Infections · Complement system · Immunoglobulins · Innate immunity



Additional supporting information may be found online in the Supporting Information section at the end of the article.

Introduction

Monoclonal antibodies are widely used nowadays as therapeutic agents, for example, in the treatment of autoimmune diseases [1, 2], cancer [3], or viral infections [4]. Additionally, antibacterial antibodies have also tremendous potential to be applied to bacterial infections, as an alternative to antibiotics in the context of rising antibiotic resistance [5, 6]. In that perspective, the activation of secondary effector functions by the monoclonal antibodies,

such as the activation of complement, remains crucial with binding by itself conferring only little bacteriostatic or bactericidal activity.

Indeed, the activation of the complement system upon antibody binding is a potent secondary effector function against various pathogenic bacteria [7–11]. Complement-mediated killing, therefore, could be an interesting pathway to be harnessed by therapeutic antibacterial monoclonal antibodies to eliminate bacterial infections. Once bound to the surface, antibodies initiate the classical pathway of complement through the recognition of their Fc domains by the complement protein C1q [12]. This triggers the sequential activation of C1r and C1s, two serine proteases

Correspondence: Dr. Jean Baudry and Dr. Klaus Eyer
e-mail: jean.baudry@espci.fr; eyerk@biomed.au.dk

associated with C1q in a complex called C1 [13]. Activation of the complement cascade ensues, resulting in inflammation [14–16], and either the opsonization of the bacteria and elimination through phagocytosis [17, 18] or the formation of a membrane-attack complex that leads to pores and osmolysis [19]. Both of these mechanisms either directly or indirectly lead to the elimination of the recognized bacteria.

A critical step for antibody-dependent complement activation is therefore the recruitment of C1q by surface-bound antibodies. C1q is a large umbrella-shaped hexameric protein, that possesses six domains that bind specifically to a region of the Fc domain of IgG or IgM antibodies, which allows C1q to bind to one IgM or several IgG antibodies present on a surface. The isotype of the antibody is essential. In BALB/c mice, IgM and several subclasses of IgG (IgG2a, IgG2b, and IgG3) have been described to activate the complement system by recruiting C1q [20]. In humans, mostly IgM and the IgG isotypes IgG1 and 3, and to a lesser extent, IgG2, were found to recruit C1q [21]. This interaction has been described for monoclonal antibodies of both isotypes using model systems, and employing these, researchers subsequently demonstrated that IgG antibodies can assemble into hexamers when their density on a surface is sufficient, which constituted the required configuration for efficient C1q docking [22–24]. Regarding IgM antibodies, recent findings showed that either pentameric or hexameric surface-bound IgM adopted a hexameric symmetry upon surface binding [25], a conformation that allowed C1q recruitment by exposing specific binding sites. These structural studies in simplified model systems have led to a better mechanistic understanding of antibody recognition by C1q, but the importance of the various crucial parameters remains unclear. Indeed, antibody-dependent C1q binding depends on several parameters beyond antibody isotype, including the affinity of the antibody for its target epitope, but also the epitope density and spatial geometry. This makes the capacity of monoclonal antibodies to recruit C1q and activate complement on complex bacterial surfaces difficult to anticipate and, therefore, generates the need to study antibody binding and C1q recruitment directly.

With that aim, we developed a direct system to characterize antibacterial antibody repertoires on the monoclonal-antibody level and quantified their capacity to recruit C1q on the bacterial surface (as the first step of the classical complement pathway) for a large diversity of IgG1, IgG2a/2b/3, and IgM antibodies. We based our system on the DropMap technology (Fig. 1A), a droplet-based microfluidic platform that enables quantitative antibody secretion measurements by compartmentalizing single cells into 50 pL droplets [26–28]. As each antibody-secreting cell (SC) only produces one variant of antibody at a time [29], the DropMap platform with its single-cell resolution studies at the single-antibody level as well. In a previous study, the characterization of bacteria-specific antibody-repertoires with single-antibody resolution was demonstrated using this system [30], where we observed that only a fraction of all secreted monoclonal antibodies were able to bind bacterial surface antigens upon exposure to said bacteria.

In the results presented herein, we aimed to gain a better understanding of the initial and defining requirements for antibody-dependent C1q recruitment onto bacterial surfaces. Due to previously published data where mice were immunized with full bacteria [30], where only a fraction of antibodies were specific for the bacterial surface, monoclonal antibodies that display the additional capacity to recruit C1q were expected scarce among the full repertoire. Therefore, we opted to study the repertoire in high throughput using the droplet array as previously described [26, 27]. In this study, we integrated a new bioassay to measure the initiation of the classical complement pathway by individual bacteria-specific antibodies through the quantification of antibody-dependent C1q recruitment, and first calibrated the assay with *P. aeruginosa* as the target bacteria. We then applied this assay to a study of antibacterial antibody responses induced by immunizing mice against *B. pertussis*, *N. meningitidis* B and C serogroup. Both bacterial species are clinically relevant as targets of vaccination in humans, and antibodies against both bacteria were known to interact with complement.

Results

Measurement of IgM and IgG secretion and IgG subclasses to detect IgG- and IgM-SCs

We employed droplet microfluidics to study the postimmunization antibody repertoires. Here, a droplet contained either a cell that secreted antibodies or not, and the bioassay components to analyze antibody secretion. The readout was based on fluorescence relocation onto magnetic nanoparticles, aligned into a vertical beadline by applying a magnetic field (Fig. 1A). The particles were functionalized to capture all potential isotypes secreted using an anti- κ light chain nanobody, and the isotype and concentration of secreted antibodies were then detected using isotype-specific, fluorescent secondary detection antibodies, thus relocating fluorescence intensity from the volume to the beadline. This resulted in an increased fluorescence intensity on the beadline relative to the rest of the droplet that could be quantified as a fluorescence relocation signal (fluorescence on the beadline against fluorescence in the droplet). Indeed, the fluorescence relocation increases with the antibody concentration in the droplet; and a calibration of the assay associated the relocation signal to an antibody concentration (Fig. 1B). This allowed to distinguish and quantify IgG and IgM secretion.

We next focused on the differentiation of the complement-inactive isotype IgG1 from the other IgG isotypes. This required modifications to the existing bioassay measuring antibody secretion [26, 27]. While the concentration of IgM and IgG antibodies was measured in parallel with a detection probe specific to each isotype in different fluorescence channels, a detection probe specific to the IgG1 subclass was added to the droplets, which allowed to further classify IgG antibodies as either IgG1, not functionally active in mice, or IgG2a/2b/3, that can activate complement (Fig. 1C, calibration in Supporting Information Fig. S1).

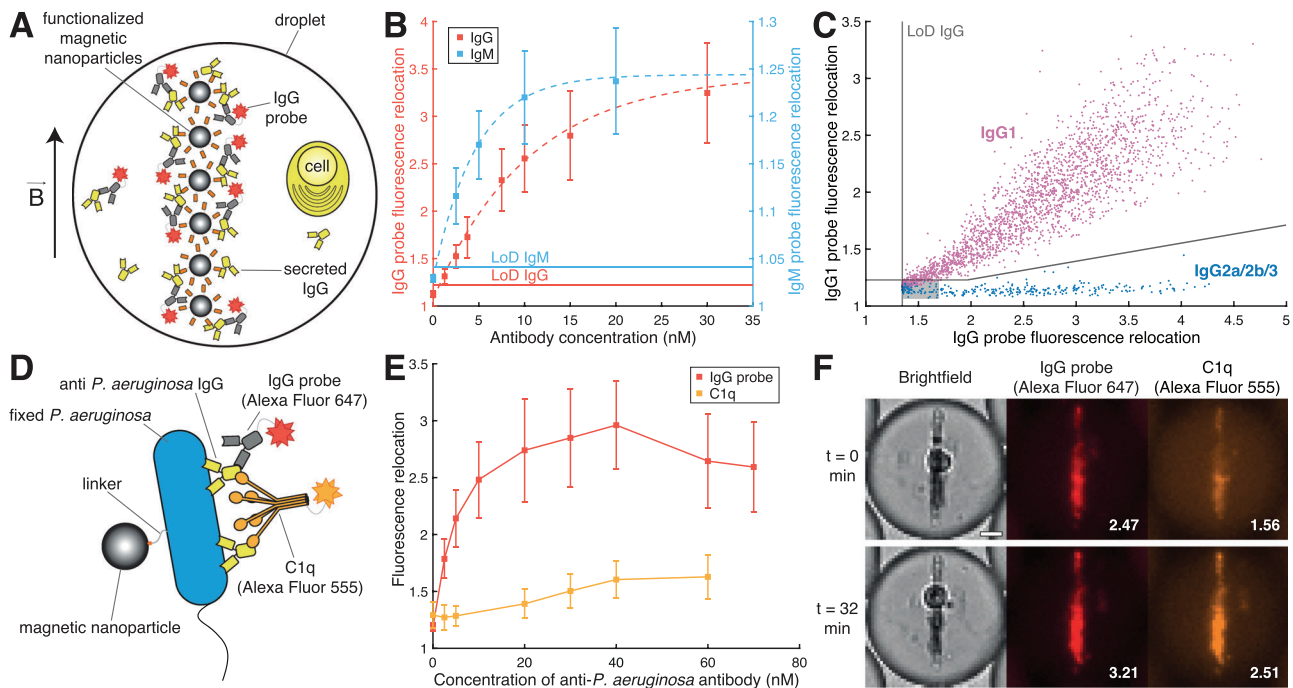


Figure 1. DropMap assays to detect secreted antibodies of different subclasses, bacteria-specific antibodies, and antibody-dependent C1q recruitment. (A) Schematic of the DropMap bioassay measuring antibody secretion. The assay for IgGs is represented here, but IgM antibodies and IgG subclasses are detected similarly using a specific probe in different fluorescence channels. Antibody secretion (yellow) is read out as the relocation of fluorescence onto the magnetic beadline. (B) Calibration curve assigning antibody concentration to the respective fluorescence relocation value for IgG in red and IgM in blue. The respective limits of detections (LoDs) are displayed with horizontal bars. (C) Data from the final timepoints in B cell experiments. Each point represents an antibody secreted by an individual splenic B cell (2,525 secreting cells in total). Antibodies with high IgG1 probe fluorescence relocation are classified as IgG1 (above the line), whereas dots underneath the line are classified as IgG2a/2b/3, see also Supporting Information Fig. S1. IgG antibodies secreted at low concentration (greyed box) are classified by visualization. (D) In parallel to the isotype, bacterial binding was assessed in a second DropMap assay. Here, the magnetic nanoparticles were functionalized with fixed bacteria (e.g. here *P. aeruginosa*) using a biotin-PEG-cholesterol linker, resulting in bacteria-coated beadlines, termed bactolines, where specific antibodies (IgM, IgG, and its subclasses, yellow) and their capability to recruit C1q were detected by fluorescence relocation. (E) Calibration curve of the bactoline assay to detect bacteria-specific antibodies activating complement, here shown with *P. aeruginosa* as the target and a control anti-*P. aeruginosa* antibody. The antibody binds to the target bacteria, and is able to recruit C1q, although only to a small proportion. (F) Example images of a droplet containing a single B cell secreting an IgG antibody binding to the target bacteria (here *N. meningitidis* C) and recruiting C1q efficiently, as detected by the fluorescence relocation for IgG and C1q on the bactoline. Scale bar = 10 μ m. If not indicated otherwise, median and standard deviations are shown. For calibration experiments, each data point corresponds to an average of approx. 15,000 to 40,000 individual droplets.

This assay was later used to identify the frequency of antibody-SCs of the respective isotypes and subclasses.

Measurement of bacteria-specific antibodies and detection of C1q-recruiting antibodies

As we were interested in specific antibacterial antibodies that were able to recruit C1q, we developed a second bioassay to selectively detect antibodies specific to a target bacteria. This assay further quantified antibody binding density on the bacterial surfaces and their capacity to trigger the classical pathway of complement by recruiting the C1q protein. To that aim, we bound inactivated bacteria on the magnetic nanoparticles of the DropMap system to use as antibody targets (Fig. 1D) [30]. Several species of bacteria were bound to the beads, *P. aeruginosa*, *B. pertussis*, and *N. meningitidis* for the study here. *P. aeruginosa* was used to calibrate the assay due to the availability of a monoclonal-specific antibody of the IgG2a subclass, and *B. pertussis* and *N. meningitidis* were used

for the experimental study. In the assays, bacteria-specific antibodies present in the droplet bound to the bacteria immobilized on the beads, and thus relocated to the beadline, here termed “bactoline”, as previously described in Heo et al. [30]. By including the same fluorescent detection probes as in the antibody secretion assay, we detected the presence of specific antibodies (positive signals in different channels) and quantified their density on the bacterial surfaces by measuring the height of the fluorescence relocation signal in the bactoline assay (presented for IgG in Fig. 1E and F, red). In addition, we integrated fluorescently labeled C1q and were also able to detect and quantify the antibody-dependent recruitment of C1q onto the bacterial surfaces (Fig. 1D). Here, if the antibody is able to recruit C1q, fluorescence relocation to the bactoline is observed in the corresponding channel (Fig. 1E and F, orange). Indeed, when employing the anti-*P. aeruginosa* IgG2a antibody and *P. aeruginosa* on the bactoline, we observed a positive correlation between IgG probe fluorescence relocation and the concentration of bacteria-specific monoclonal antibody (Fig. 1E, red), also linked to a small but quantifiable increase in

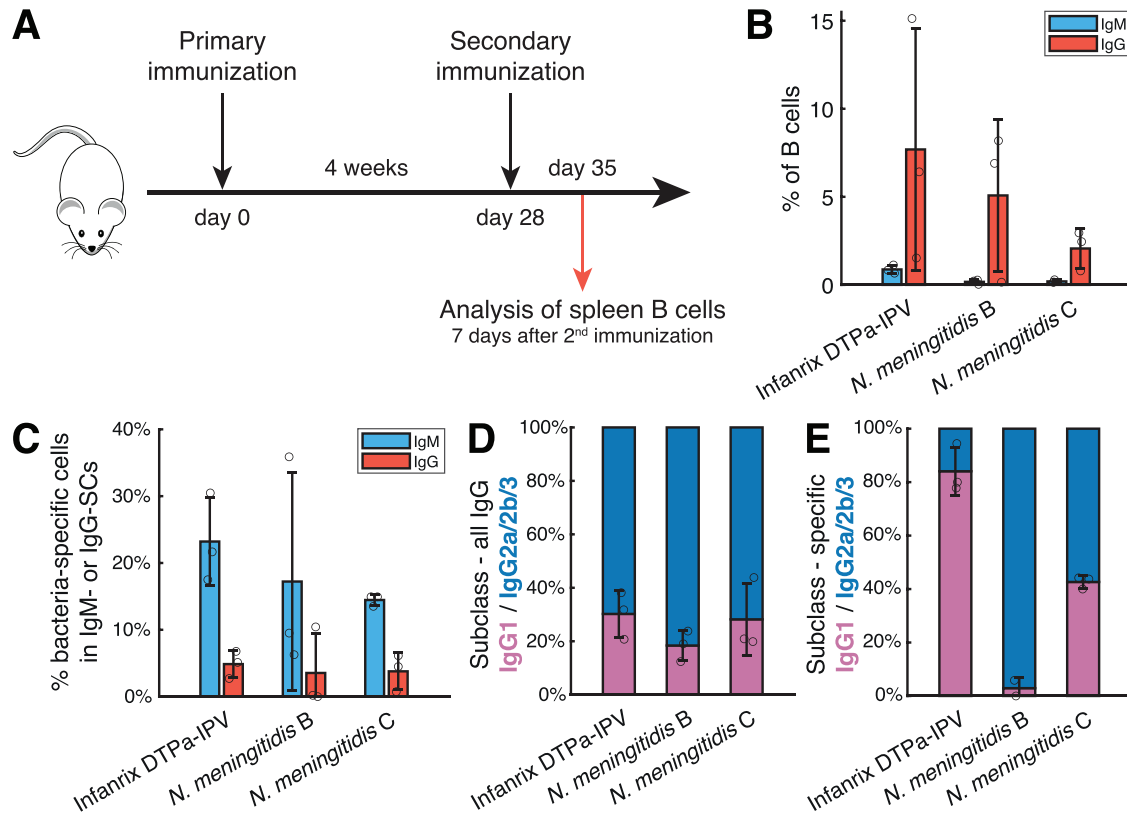


Figure 2. Description of the induced humoral immune responses in mice following immunizations with a commercial vaccine or inactivated bacteria. (A) Schedule of mice immunizations and harvest of spleen B cells for the analysis using the described bioassays. (B) Frequencies of IgM- and IgG-SCs within the purified splenic cells from B cell lineage in mice immunized twice with either DTPa-IPV vaccine (control vaccine, including acellular pertussis components) or fixed *N. meningitidis* from the B or C serogroup. (C) Percentages of IgM- or IgG-SCs secreting an antibody specific to the target bacteria (either *B. pertussis*, *N. meningitidis* serogroup B or C, respectively), measured with the bactoline assay (Fig. 1D). (D and E) Further grouping of the IgG-secreting cells into IgG subclass, classified as IgG1 or IgG2a/2b/3, either for (D) all IgG-SCs or (E) bacteria-specific IgG-SCs. $n = 3$ for all, mean and standard deviations are shown.

C1q relocation (Fig. 1E, orange). The increase in C1q relocation is due to recruitment by the anti-*P. aeruginosa* antibody, and not by the secondary IgG detection antibody that was selected to not bind C1q by itself. It was also previously shown that a nonspecific IgG does not lead to any increase in IgG relocation [30]. Therefore, the second assay that we developed was able to analyze antibody repertoires at the single-cell level with the high throughput enabled by the DropMap platform, quantifying the frequency of bacteria-specific antibodies, their individual maximal binding density on target bacteria (IgM or IgG) and their ability to bind and relocate C1q.

Immunization with full bacteria led to a corresponding immune response containing surface-specific antibodies

To induce the antibody responses for our study, we immunized mice, following the schedule displayed in Fig. 2A, to prompt specific antibody responses against either *B. pertussis* or *N. meningitidis* B or C serogroup. Initially, *P. aeruginosa* was also included in this study but the immunized mice did not respond to immunization

by generating specific IgG-SCs. This was also in agreement with previous studies using a heat-killed version of said bacterium [30]. To elicit antibody responses targeted against *B. pertussis*, we used a reduced dose of the vaccine Infanrix DTPa-IPV, a tetravalent acellular vaccine that includes two *B. pertussis* surface protein antigens, filamentous hemagglutinin, and pertactin, as well as other antigens corresponding to different vaccination targets not relevant for our study. Regarding the antibody responses against *N. meningitidis*, we chose to immunize mice directly with paraformaldehyde-fixed *N. meningitidis* bacteria, either from the B or C serogroup, identical to the bacteria present on the nanoparticles in the *N. meningitidis*-specific antibody detection assay (same batch).

The commercial vaccine resulted in a large general antibody-SC response in the spleen (Fig. 2B), probably owing to the variety of antigens included in its formulation. The IgG response was especially induced, although at a variable extent between the individual mice of the group, with frequencies of IgG-SCs ranging from 1.5 to 15% of the splenic B cells and an average of $7.7 \pm 6.9\%$ ($n = 3$). In addition, we detected $0.88 \pm 0.24\%$ of IgM-SCs. In terms of binding toward fixed *B. pertussis*, $23.2 \pm 6.6\%$ of the IgM-SCs and, interestingly, only $4.9 \pm 2.0\%$ of the IgG-SCs were

specific for the bacteria (Fig. 2C). Due to the use of the commercial vaccine containing two surface antigens, the vast majority of specific antibodies are expected to either target the filamentous hemagglutinin or the pertactin of *B. pertussis* since those are the surface antigens contained in the Infanrix vaccine. The different and lower frequency of specific cells among isotype-SCs might be explained by the nonrelevant antigens contained in the vaccine or differences in their efficiency to induce class-switching.

The immunizations with fixed *N. meningitidis* also induced a general antibody response with dominant IgG-SCs (Fig. 2B). Within splenic B cells, the serogroup B immunizations resulted in $5.1 \pm 4.3\%$ IgG- and $0.17 \pm 0.13\%$ IgM-SCs ($n = 3$), while the serogroup C immunizations resulted in $2.1 \pm 1.1\%$ IgG- and $0.20 \pm 0.08\%$ IgM-SCs ($n = 3$). Surprisingly, for both conditions, the fraction of the bacterial surface-specific IgG was low, on average below 5% of the IgG-SCs (Fig. 2C), but similar to the vaccination with commercial antigen. This could also be due to the variety of antigens present in the bacteria, where only a small fraction will be available on the surface. Also here, 3.8 (for serogroup B) and 4.9 (for serogroup C) times higher frequency of surface-recognizing antibodies were observed within IgMs compared with IgGs. Still, we detected bacteria-specific IgM- and IgG-SCs for all animals except one and even observed a particularly large response for one of the mice immunized with *N. meningitidis* B, with 394 specific IgG-SCs detected out of the 46,000 B cells that we measured. Therefore, we concluded that, although rare, we would have enough positive events to study C1q recruitment in more detail.

The isotype and subclass composition of the antibody repertoires are critical for the binding of C1q and initiation of the complement cascade. Regarding the IgG isotype, the general responses were mostly composed of potentially complement-activating isotypes IgG2a, 2b, or 3 for all three conditions (Fig. 2D). Interestingly, when focusing only on bacteria-specific IgG antibodies, the percentages within the IgG subclasses were different between conditions (Fig. 2E). The DTPa-IPV immunizations resulted in mostly specific IgG1-antibodies ($84 \pm 9\%$ IgG1), while the *N. meningitidis* B immunizations resulted in almost entirely IgG2a/2b/3 subclasses ($97 \pm 4\%$ IgG2a/2b/3). The antibody responses to *N. meningitidis* C immunizations were more balanced in that regard, with $57 \pm 2\%$ of the bacteria-specific antibodies within the potentially activating IgG2a/2b/3 subclasses. Therefore, we concluded that both immunizations with *N. meningitidis* subgroups might allow us to study C1q recruitment by IgG antibodies and its requirements due to the presence of a good fraction of antibodies of interest, whereas such an event would be even rarer or even completely absent in the immunization with *B. pertussis* due to the prevalence of the IgG1 isotype.

High-surface density of IgG2a/2b/3 as necessary requirement for C1q recruitment

After confirming that there were surface-specific antibodies generated in our immunizations, we assessed whether the surface-

binding bacteria-specific antibodies were able to initiate the classical complement pathway on the fixed bacteria by using the second presented bioassay, looking first at IgG. This was done with samples from the same cell solutions in parallel. While not exactly performed on the same cells, but cells from the same sample, we would expect a similar frequency of surface-specific antibodies being secreted.

For the group of three mice immunized with the Infanrix vaccine, we detected in total of 180 individual *B. pertussis*-specific IgG-SCs. For these antibodies, we measured the binding density of the secreted IgG antibody on the surfaces of the target bacteria present in the detection assay (see bacteriology assay above), as well as the potential recruitment of the C1q protein to the bacterial surface. The antibodies were afterward represented as a scatter plot of their C1q binding density against their IgG binding density, as shown in Fig. 3A, and further color-stained for their subclass category. Interestingly, none of the *B. pertussis*-specific IgG antibodies triggered C1q binding at a detectable level. However, as mentioned before, only a few IgG2a, IgG2b, or IgG3 were found among the *B. pertussis*-specific IgG-SCs (36/180, 20%), and most antibodies of this isotype only recognized epitopes present at a low density on the bacterial surface. Indeed, we observed only a handful of cells secreting a *B. pertussis*-specific IgG binding with a high density (see methods for definition) on the surfaces of the fixed bacteria (24/180 specific IgGs, 13.3%). All of these antibodies were of the IgG1 isotype that is unable to interact with C1q. This finding might reflect a low surface abundance of the two target antigens contained in the vaccine (filamentous hemagglutinin and pertactin), a defect in the ability to switch for these antigens to IgG2a/2b/3 isotypes, or alternative mechanisms present on the bacteria preventing binding. In short, this experiment agreed with our expectations that the monoclonal complement-initiating antibodies might be absent in our selected *B. pertussis* immunizations.

For *N. meningitidis* (Fig. 3B and C), we successfully detected C1q-binding (C1q⁺) IgG antibodies against both serogroups of the target bacteria. Indeed, for the mice immunized with the C serogroup of *N. meningitidis*, we observed 10 IgG-SCs that induced IgG-dependent C1q binding out of the total 64 specific IgG-SCs detected (Fig. 3B), representing 15.6% of the bacterial surface-specific IgGs. For the mice immunized with fixed *N. meningitidis* B, we detected 17 C1q⁺ IgG-SCs out of the 397 bacteria-specific IgG-SCs (4.2%, Fig. 3C). As expected from previous literature, only specific IgGs of the IgG2a/IgG2b/IgG3 subclasses engaged C1q, and no C1q⁺ IgG1 was observed in either, even when bound at a high density. Focusing on the C1q⁺ events, only high-density IgG2a/2b/3 antibodies allowed for the binding of C1q (except one low-density IgG against *N. meningitidis* B, only slightly above the detection threshold), indicating that high density was necessary for efficient C1q recruitment. Interestingly, it seemed that density alone was not always sufficient, as we observed one monoclonal high-density IgG2a/2b/3 in the B serogroup immunization that was not able to do so (Fig. 3C). Additionally, we observed heterogeneity in their capability of recruiting C1q, indicated by the large variation on the y-axis within a similar range on the x-axis. In general, the recruitment of

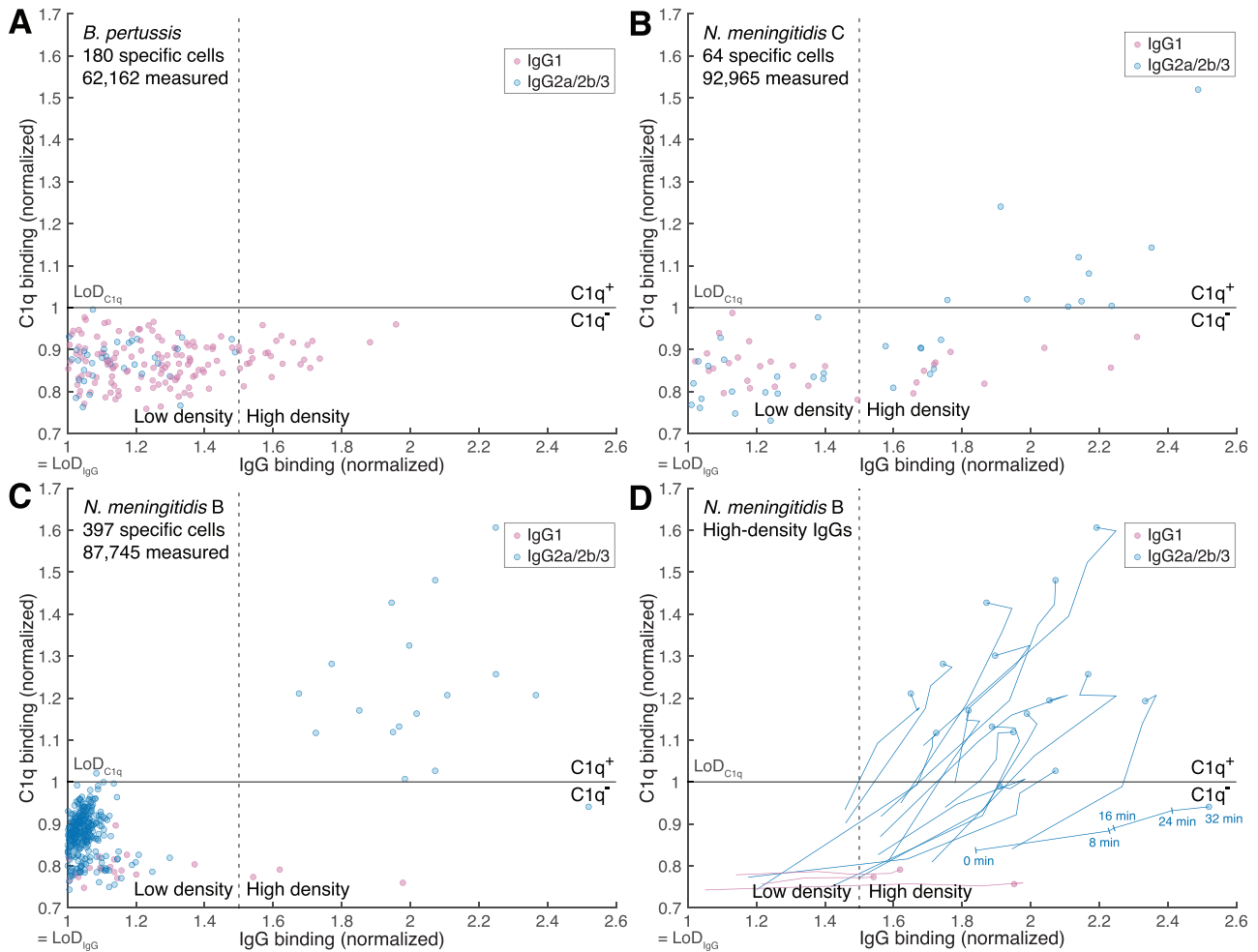


Figure 3. C1q binding was restricted to a small subpopulation of secreted, monoclonal IgG2a/2b/3 antibodies and was linked to density. (A) *B. pertussis*-specific IgG-SCs (180 in total out of 62,162 B cells measured), pooled from measurements of three mice immunized with Infanrix DTPa-IPV. (B and C) Specific IgG-SCs pooled from measurements of three mice immunized with fixed *N. meningitidis*, either (B) from the C serogroup (64 cells out of 92,965 B cells measured) or (C) from the B serogroup (397 cells out of 87,745 B cells). In all three, each dot corresponds to an antibody secreted by an individual cell; the x-axis corresponds to the maximum relocation signal of the anti-IgG probe (i.e. IgG binding density) measured over the duration of the measurement (normalized by the LoD of IgG, see methods), the y-axis to the maximum relocation signal of C1q measured over the duration of the measurement (normalized by the LoD of C1q binding). The dotted line illustrates an arbitrary limit to differentiate between low- and high-density IgG binding. (D) The high-density *N. meningitidis* B-specific IgG antibodies from panel C were isolated and the individual traces of C1q binding against IgG binding over the duration of the measurement were plotted in this panel. Time stamps are shown next to one of the traces, each trace represents a monoclonal IgG secreted by an individual cell, and the dots represent the final time point of each trace.

C1q onto bacteria from the *N. meningitidis* serotype C seemed lower at similar densities compared with the B serotype.

Since we measured the IgG and C1q relocation signals over time, also the dynamics and evolution of C1q binding against IgG binding could be represented throughout the measurements, displayed in Fig. 3D. On this graph, we displayed only the high-density IgG antibodies against *N. meningitidis* serogroup B, as the low-density IgGs did not display any interesting dynamics. The obtained traces exhibited a mostly linear relationship after a certain point on the x-axis (i.e. density) up to the point until the IgG binding signal reached a plateau, likely due to the saturation of all the target epitopes available on the surfaces of the fixed bacteria. The upper left quadrant, representing low density/C1q⁺, was not explored or crossed by any trace of a monoclonal IgG, indi-

cating that a high density of functionally active IgG2a/2b/3 was necessary to recruit C1q in our experimental setting. The slope was close to zero for the specific IgG1 antibodies, again reflecting an absence of C1q relocation due to the inability of said isotype to do so.

To summarize, we observed in these different experiments that IgG-dependent C1q binding was almost exclusively reserved to IgGs binding at a high density on the target bacteria, and only to antibodies of the functionally active IgG2a/2b/3 subclasses. Additionally, we observed that a high-binding density of IgG2a/2b/3 on the bacterial surface was almost exclusively sufficient to induce C1q recruitment, as most high-density bound IgGs of those subclasses also displayed antibody-dependent C1q binding in these experiments.

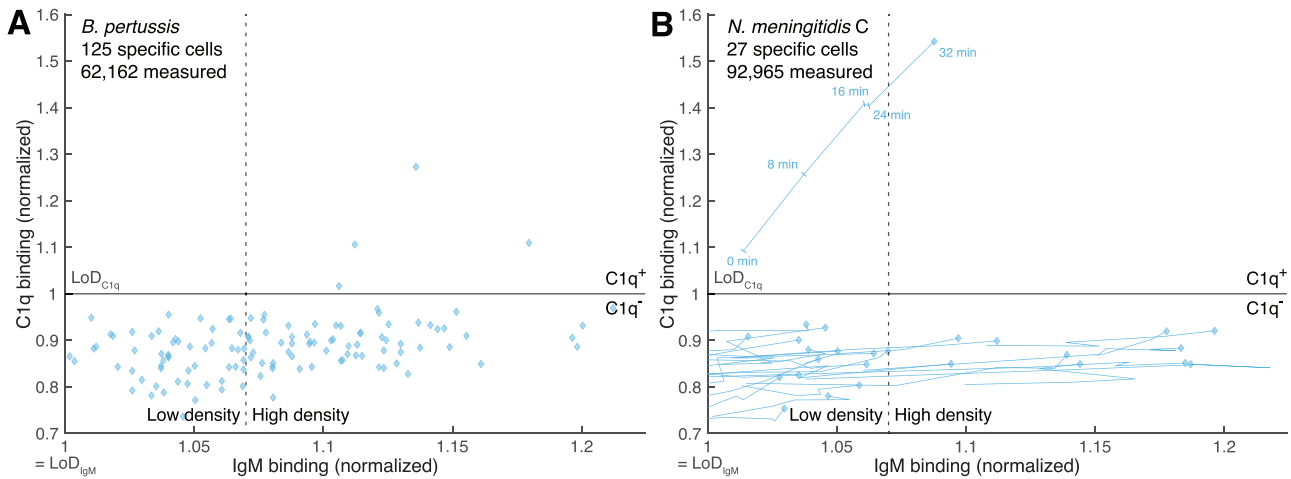


Figure 4. C1q binding by monoclonal IgM antibodies was rare, and seldomly linked to binding density. (A) *B. pertussis*-specific IgM-SCs (125 in total out of 62,162 B cells measured), pooled from measurements of three separate mice immunized with Infanrix DTPa-IPV. Each dot corresponds to a monoclonal antibody secreted by an individual cell. The x-axis corresponds to the maximum relocation signal of the anti-IgM probe (i.e. IgM binding density) over the duration of the measurement (normalized by the LoD of IgM, see methods), the y-axis to the maximum relocation signal of C1q measured over the duration of the measurement (normalized by the LoD of C1q binding). Cells with a C1q binding value above 1 are classified as C1q-binding (C1q⁺). An arbitrary limit between low- and high-density IgM binding was placed. Only high-density IgMs relocated C1q to the bacterial surface, but a high density of IgM was not sufficient to relocate C1q. (B) *N. meningitidis* C-specific IgM-SCs (27 out of 92,965 B cells measured), pooled from measurements of three mice immunized with fixed *N. meningitidis* serogroup C, represented as in panel A. Additionally, traces representing the evolution of C1q binding against IgM binding over the full duration of the measurement are plotted here. Time stamps are shown next to one of the traces, and the dots represent the final time point of each trace. Here, only one IgM antibody could recruit C1q, however, starting at a low IgM binding density.

C1q recruitment was rarely triggered by IgM antibodies, even bound at high density

We lastly looked in detail at the bacteria-specific IgM-SCs detected against the different model bacteria. We analyzed these events in the same way as the specific IgG-SCs, comparing this time the IgM binding density on the target bacterial surfaces to the IgM-dependent C1q binding density.

For the mice immunized with the DTPa-IPV vaccine, the obtained *B. pertussis*-specific cells are represented in Fig. 4A. For this condition, we detected 125 specific IgM-SCs, secreting antibodies bound at various densities on the bacteria, with 46% of IgMs binding at what we deemed low density, and 54% at a high density. Here, four of the specific IgM antibodies were classified as C1q⁺ as they recruited C1q onto the surface of *B. pertussis*. Also, we observed that only IgM antibodies binding with a high density were able to relocate C1q, although the value of this observation remains questionable due the low number of positive events. However, and more interestingly, a high density of surface-bound IgM was not an efficient descriptor and correlate for C1q recruitment, as only four out of the 68 IgM antibodies binding with a high density showed detectable C1q binding, only representing 6% of the total specific IgM.

The immunizations with fixed *N. meningitidis* from the B or C serogroups led to even fewer specific IgM-SCs compared with the DTPa-IPV immunizations. In total, we could detect only 17 *N. meningitidis* B-specific IgM antibodies, and 71% of these specific IgMs bound the bacteria with a high density (Supporting Information Fig. S2A). Consistent with the low occurrence of C1q-binding

IgM observed in the *B. pertussis* samples, we detected no C1q⁺ monoclonal IgM in this condition. This could also be due to the low number of events in general, but it is interesting to note that, while high-surface density IgM were present, none of these led to C1q recruitment. For the mice immunized with fixed *N. meningitidis* of the C serogroup, the number of specific IgM-SCs was slightly higher (27), and we could detect one IgM bound at high density that relocated C1q to the surfaces of the bacteria efficiently (Supporting Information Fig. S2B). Following this event over time, we observed a perfectly linear trend for the sole positive C1q-recruiting IgM (Fig. 4B, $R^2 = 0.994$), this time also crossing the low density–C1q⁺ quadrant. Indeed, the antibody seemed very efficient with already detectable C1q recruitment at the first time point when the density of bound IgM was still low.

In summary, the results using *N. meningitidis* as a target bacteria confirmed our observation with the *B. pertussis*-specific IgMs, namely that a high density of bound IgM antibody was important but not sufficient to efficiently recruit C1q in this experimental setting. In that regard, IgM displayed a distinct behavior compared with the functionally active subclasses of IgG, where a high density of bound antibodies seemed to be the only requirement in most cases for C1q recruitment.

Discussion

In these experiments, we were interested in understanding the important parameters of monoclonal antibody binding to a bacterial surface necessary to initiate the classical complement

cascade, here assayed by its first step only, C1q recruitment. We further specifically focused on epitope and antibody density in our study. While screenings for monoclonal antibacterial antibodies are often performed to select high-affinity antibodies, we aimed to focus on the surface density of the antibody, which will be a mix between its affinity or avidity, concentration, and, most importantly, the epitope density on the surface. While the first two parameters can be somewhat optimized during development, the latter represents a clear limitation and, due to its nature, was best analyzed in a direct manner.

Therefore, we had to generate an assay that allowed us to investigate this parameter and scientific question on the monoclonal antibody level. The results described here demonstrate that our assay was able to detect either IgM or IgG and quantify the C1q-binding potential of single bacteria-specific antibodies. Furthermore, IgGs were differentiated into IgG1 or IgG2a/2b/3 to distinguish complement active from the inactive IgG1 subclass. We also correlated C1q recruitment to the antibody density on the surface, generating an observational parameter linked to the C1q-recruitment efficiency of the monoclonal antibody. We have shown that our assay was able to detect IgM and IgG antibodies binding C1q protein and distinguish subtle details in their efficiency to do so, although the frequency of such events was very low. As an example, on average only 1 out of 314 IgG-SCs secreted a C1q⁺ IgG after the *N. meningitidis* B immunizations. For this reason, a high-throughput method was necessary to search for complement-activating antibodies against the used target bacteria.

A clear limitation of the current setup lies in the use of the first step of the classical complement cascade, C1q recruitment, only. We considered here C1q recruitment by antibodies as a proxy for complement activation — we were not able to measure activation further down in the complement cascade, and no additional complement proteins were present in the assay. However, current literature suggests a strong link between C1q binding and complement activation, although the efficacy of this link might vary for different antibody isotypes at similar densities [31–34]. On the other hand, C1q binding itself is also influenced by additional factors. The C1r/s proteases, associated with C1q in the C1 complex, have been described to modulate C1 binding and were not present in the assay [31]. Therefore, our assay offers limited insight into the complex mechanism regulating C1q binding. Another limitation lies in the use of fixed bacteria. The fact that the bacterial surfaces are fixed by crosslinking with paraformaldehyde in our experiments, although as mild as possible to ensure killing, might alter surface epitopes, their availability, and also limit their rearrangement and diffusion within the membrane. Consequently, this may also add additional geometrical constraints, therefore, reducing the frequency of C1q-recruiting antibodies. Another limitation of this study lies in the absence of more commercial monoclonal antibodies that could be used for calibration (only one IgG antibody against a different bacterial species, *P. aeruginosa*, Fig. 1E). Their availability would enable a better quantification and comparison of C1q recruitment across different cell populations and immunizations.

Nonetheless, our system allowed us to link several fundamental antibody parameters to the C1q-recruitment efficiency of the bacteria-specific antibodies. First, we confirmed that the IgG subclass is a defining parameter in this interaction. We observed that IgG1 antibodies were not able to recruit C1q, even at a high density on the surfaces of the bacteria (Fig. 3). This is in agreement with previous reports showing that the murine IgG1 subclass induced only very weak to undetectable activation of the classical pathway of complement [35–38]. In our experiments, no IgG1 was above the limit of detection that we set for positive C1q recruitment, and over time, their recruitment slopes were close to zero, showing no increase in concentration. However, a few IgG1 antibodies, in particular, bound at a high density, had a C1q binding signal close to that limit (e.g. see Fig. 3A), which might reflect the very weak but non-zero C1q-binding capacity of some IgG1 antibodies described before [37, 38].

On the other hand, we detected C1q binding induced by monoclonal IgM and the IgG subclasses IgG2a/IgG2b/IgG3. Interestingly, for the IgG subclasses, a high density of surface-bound antibodies seemed to be necessary for antibody-dependent C1q binding (Fig. 3). Accordingly, we did not observe any C1q⁺ IgG antibodies against *B. pertussis*, as all high-density IgGs were of the IgG1 subclass in that case (Fig. 3A). In immunizations with *Neisseria*, a high density of IgG2a/2b/3 was mostly sufficient for C1q recruitment, as the large majority of IgG2a/IgG2b/IgG3 at a high surface density were C1q⁺ (Fig. 3B–D). The importance of a high density of antibodies bound to the pathogen surface for efficient classical pathway activation has been described before for IgG antibodies of various species [39, 40]. The reason for this density requirement is that the C1q protein only has a very low affinity for a single IgG Fc domain and needs to bind to several IgG Fc domains at once. Earlier models proposed that the C1q protein should bind to the Fc domain of at least two IgG antibodies, each binding surface antigens with both of their Fab domains. However, more recent studies have proposed that efficient C1q binding would instead require six IgG antibodies nearby [22–24]. Diebolder et al. described that six IgG molecules binding to antigens on a model surface assembled in a hexameric shape through noncovalent interactions between their Fc domains, forming a circular Fc platform on top with six C1q-binding domains available, on which the C1 complex can dock with high avidity to initiate the classical complement cascade. In the IgG hexamer, each of the IgG molecules is bound to the surface with only one of its two Fab arms, allowing for little avidity. Indeed, this hexameric assembly of IgG antibodies seems to be the main efficient mechanism for C1q binding by IgG antibodies [22].

In agreement with this observation, the requirement for six specific IgGs to bind in close proximity might also explain the threshold in IgG density that we observed in our experiments (Fig. 3), with only high-density binding IgGs leading to detectable levels of C1q relocated on the bacterial surfaces. This might also be linked to the physical range of C1 itself [41, 42]. In our experiments, we found a quasi-linear increase after an initial lag phase. Below this IgG density threshold, it seems unlikely that sufficient IgG antibodies were available in close proximity to assemble in

a hexamer and recruit C1q efficiently. In addition to the threshold in IgG density required to initiate C1q binding, the maximum density of antibody-dependent C1q binding attainable depended linearly on the density of bound IgG, both for *N. meningitidis* B and C (Fig. 3B and C), which would be linked to an increased likelihood to form IgG hexamers as the IgG density increases past the threshold. Therefore, our experiments underlined the importance of antibody density on a bacterial surface if the complement is supposed to mediate bactericidal effects — this observation is crucial when selecting antigen targets on the bacterial surface.

However, while for a given clone the correlation between density and C1q recruitment is excellent, this response is antibody-dependent: we observed similar IgG binding values leading to very different C1q-binding activities for the various monoclonal IgGs detected (e.g. Fig. 3C). An obvious first parameter that could be at play here would be the exact subclass of the IgG antibody. Indeed, in our experiments, we could not distinguish between the mouse IgG2a, IgG2b, and IgG3 subclasses that can all activate the classical complement pathway, and experiments with human antibodies have shown that this might influence C1q binding signal [31]. These three murine subclasses were reported to have different thresholds and efficacies to induce complement activation [35–37], most likely due to varying C1q recruitment efficiency, since it is the first step of the complement cascade where the antibody plays a major role. Another parameter influencing the C1q-binding efficiency of C1q⁺ IgGs in our experiments could be the target antigen and the recognized epitope. Since we used full fixed *N. meningitidis* for the immunizations, the complete diversity of bacterial antigens was available for the affinity maturation of the antibody-SCs, and thus the specific *N. meningitidis*-IgG-SCs that we detected (Fig. 3B and C) could be targeting very different surface antigens and also different epitopes within the antigens. Various studies have reported before that potent complement activation depended on antigen and epitope-specific parameters, such as the orientation of bound IgGs due to epitope geometry [43–45], the fluidity of the antigen on the cell membrane [44–46], the proximity of the target epitope to the cell membrane [47–49] or the off rate k_{off} of bound IgGs [46]. A simple interpretation of those findings is that all of these different factors impact the formation of the hexameric IgG assembly, leading to more or less efficient C1q docking and explaining the differences in C1q binding efficiency observed in our experiments, although we cannot attribute those differences to specific parameters here.

Regarding IgM antibodies, we observed that in contrast to IgG, a high density of bound IgM was not sufficient for efficient C1q recruitment. Indeed, for all three of the bacterial models studied here, only a few or none of the specific IgM could recruit C1q at a detectable level despite the detection of IgM antibodies binding at a high density (see for example Fig. 4A, only 10% of the high-density IgMs were C1q⁺). In addition, we also observed C1q recruitment starting at low IgM density for one particularly efficient IgM antibody (Fig. 4B), contrasting with the antibody density threshold for C1q binding that we observed for IgG. The structural properties of the antigen-IgM-C1 complex could explain this phenomenon. The IgM assembly has been described as either

pentameric [50] or, less frequently, hexameric [51]. Furthermore, studies have shown that the assembly underwent a conformational change from a mostly planar shape in solution to a staple-like shape when bound to surface antigens [52], exposing binding sites that would allow C1q docking. The structure of IgM bound to antigen and in complex with the C1 protein has been recently resolved using electron cryotomography [25], which revealed that both pentameric and hexameric IgM formed an equivalent C6-symmetric hexameric structure in that complex. Thus, the structure of the IgM-C1 assembly was described to be very similar to that of the IgG hexamer that enables efficient C1q binding for both IgM forms [22]. Additionally, the study showed that all Fab arms of IgM engaged with the surface antigens in the IgM-C1 assembly. For each IgM monomer, both Fab domains were bound, leading to avidity.

Interestingly, we observed that, even at high density, only very few IgM were positive for C1q recruitment. While we are not certain of the mechanism behind this observation and its power is limited by the few surface-specific IgMs found, our current hypothesis to explain this finding lies in the rather strict geometrical constraints of the IgM-C1q assembly [24, 53]. Only certain epitopes may fulfill these conditions, for instance, requiring not only a high antigen density but also a specific location and orientation of the binding site on the target epitope. This would explain that only a few detected bacteria-specific IgM antibodies recruited C1q, but additional experiments are needed to clarify this point. However, it seems that when targeting an adequate epitope, monoclonal IgM antibodies were able to recruit C1q with an efficiency exceeding that of highly efficient IgG antibodies (Fig. 4B). In summary, these results and observations further illustrate the complexity of the IgM-complement recruitment cascade, suggesting that monoclonal IgM development might be a complex format for the generation of antibacterial antibodies, and that complement initiation by IgM might be conferred by a polyclonal mixture and not a monoclonal species *in vivo*.

We highlighted here that a high density of bound IgGs was necessary for optimal C1q recruitment and therefore a first requirement when developing complement-activating monoclonal antibodies is to make sure that they target surface antigens present at a high density. However, we also showed here that it would not be sufficient to select antibodies based on very high affinity and target epitope density to find efficient activators of the complement system. Instead, it is crucial to also measure subsequent C1q binding. Indeed, only a few IgM antibodies were able to bind C1q and although most functionally active IgGs relocated C1q, they did so with widely varying efficiency. This validates our approach that allows a fine quantification of an antibody's potential to induce C1q binding. The results of our study point to IgG antibodies targeting antigens present at a high density as ideal monoclonal therapeutic antibody candidates, rather than IgM antibodies that were not often able to recruit C1q even when binding at high densities. To be evaluated as a potential therapeutic, these murine antibodies would need to be reformatted into a complement-activating human IgG subclass. In this context, even a high-density murine IgG1 might provide value as this isotype could be exchanged.

In the context of rising antibiotic resistance, our findings could be applied to the development of new complement-activating antibacterial antibodies to be used as therapeutic alternatives to antibiotics. Lastly, the developed assay measuring and quantifying antibody density and C1q binding in parallel might have different applications in various diseases where complement-activation is either observed as a feature or could be used as a therapeutic strategy – in inflammation, cancer, or autoimmunity [54].

Methods and materials

Immunization of mice

For immunizations against *B. pertussis*, we used a commercially available vaccine (Infanrix DTPa-IPV, GlaxoSmithKline). For immunization with *Neisseria*, we used *N. meningitidis* bacteria (10^8 cells per immunization), either from the serogroup B (ATCC strain 13090) or C (DSMZ strain 15464), inactivated by fixation with paraformaldehyde (Fluka). Before immunization, the absence of bacterial growth was tested, that is, their inactivation was confirmed. All the fixed bacteria solutions were prepared in PBS (Gibco) and mixed 1:1 with 2% Alhydrogel adjuvant (alum, Invivogen). Eight-to-ten-week-old female BALB/c mice (Janvier, three animals per experimental condition) were immunized with 100 μ L of either the vaccine (one-fifth of the human dose) or fixed bacteria i.p. Each mouse was immunized a second time 4 weeks later with the same antigen solution. On day 7 after secondary immunization, the experiment terminated and the spleen was harvested.

Aqueous phase I for droplet generation: preparation of cells or control antibody solutions

Aqueous phase I contained either purified monoclonal antibodies for calibration experiments or a B-cell suspension for cellular measurements. The calibration antibodies used are listed in Supporting Information Table S1. For cell measurements, single-cell suspensions were prepared from the extracted spleens and then enriched in B cells using the Pan B Cell Isolation kit II (mouse) and a MultiMACS device (both Miltenyi Biotec). The isolated B cells were centrifuged at $400 \times g$ for 5 min at 4°C, then the cell pellet was gently resuspended in cell medium to achieve a concentration of 10 million cells/mL. In order to minimize antibody secretion in bulk, the cell suspension was prepared just before droplet generation and kept on ice for short-term storage. The cell medium was composed of RPMI 1640 without phenol red (Sigma-Aldrich, R7509), supplemented with 5% KnockOut Serum Replacement (Thermo Fisher, 10828010), 0.5% recombinant human serum albumin (Sigma-Aldrich, A9731), 25 mM HEPES (Thermo Fisher, 15630080) and 0.1% Pluronic F-127 (Thermo Fisher, P6866), and filtered sterile.

Aqueous phase IIA for droplet generation: preparation of the antibody secretion assay

For the antibody secretion assay, aqueous phase II contained streptavidin-coated paramagnetic nanoparticles (Ademtech, 03232) functionalized with biotin anti-murine kappa light chain V_HH (Thermo Fisher, 7103152100) as described in detail elsewhere [27]. The particles were resuspended in a cell medium at 50% of their stock concentration. Afterward, anti-mouse IgG Fc Alexa Fluor 647 (SouthernBiotech, 1033-31), Zenon Alexa Fluor 488 mouse IgG1 labeling kit (Thermo Fisher, Z25002) and AffiniPure F(ab')₂ Fragment Anti-Mouse IgM, μ chain specific, DyLight 405 labeled (Jackson ImmunoResearch, 715-476-020) were added at 75, 50, and 75 nM final in-droplet concentrations, respectively.

Aqueous phase IIB for droplet generation: preparation of the bactoline assay

For the bactoline assay, aqueous phase II contained streptavidin-coated paramagnetic nanoparticles (Ademtech, 03232) functionalized with paraformaldehyde-fixed bacteria, either *P. aeruginosa* (ATCC 10145) for the calibration experiments or *B. pertussis* or *N. meningitidis* for the cell measurements (species and strain listed above). Per 100 μ L final aqueous phase II volume, either 100 μ L fixed *P. aeruginosa* solution, 50 μ L fixed *B. pertussis* solution, or 15 μ L *N. meningitidis* solution, each at OD₆₀₀ = 20, were centrifuged ($4000 \times g$, 5 min, 4°C). The supernatant was discarded and the bacteria were resuspended in 20 μ L of PBS with 1 mM biotin-PEG-cholesterol (Nanocs, PG2-BNCS-3k) and incubated overnight at 4°C. The bacteria were then washed 4 times with 1 mL PBS before resuspension in 50 μ L PBS with streptavidin-coated paramagnetic nanoparticles at their stock concentration. The mixture was incubated on a horizontal shaker (ThermoMixer C Eppendorf, Fisher Scientific, 13527550) for 2 h at 4°C and 850 rpm. Following this, the nanoparticles were collected using a magnet and washed to remove unbound bacteria. The nanoparticles were then resuspended and incubated in 100 μ L cell medium for 30 min on ice to block nonspecific binding, washed again, and resuspended in 100 μ L cell medium (50% of their stock concentration). Afterward, anti-mouse IgG Fc Alexa Fluor 647 (SouthernBiotech, 1033-31), Zenon Alexa Fluor 488 mouse IgG1 labeling kit (Thermo Fisher, Z25002), and AffiniPure F(ab')₂ Fragment Anti-Mouse IgM, μ chain specific, DyLight 405 labeled (Jackson ImmunoResearch, 715-476-020) and C1q from human serum (Sigma-Aldrich, C1740, labeled in-house with Alexa Fluor 555 using amine-reactive labeling) were added at 45, 30, 45, and 5 nM final in-droplet concentrations, respectively.

Generation of droplets and chamber filling

Water-in-oil emulsion droplets containing a 50/50% mix of aqueous phase I and either aqueous phase IIA for the antibody secre-

tion assay or aqueous phase IIB for the bactoline assay were generated using a custom-made PDMS microfluidic chip as described elsewhere [27]. The droplets were directly transferred from the chip outlet into a 2D glass observation chamber (described in ref. [27]) via a PTFE tubing (Fisher Scientific, 11919445) passing through a ring magnet (Amazing Magnets, H250H-DM). Once the chamber was filled with the droplets, it was closed and mounted onto a fluorescence microscope for imaging.

Cell measurements

The splenic B cells were analyzed using the DropMap platform and the assay to measure antibody secretion and isotype. In parallel, a different aliquot of the splenic B cells was also analyzed with the DropMap bactoline assay to detect bacteria-specific antibodies and their potential to activate the classical complement pathway. For each of the bactoline measurements, the magnetic beads were coated with paraformaldehyde-fixed bacteria corresponding to the bacterial species that the analyzed mouse was immunized against. We used fixed *B. pertussis* (DSMZ strain 4923) for the mice immunized with Infanrix DTPa-IPV and fixed *N. meningitidis* serogroup B or C for each *Neisseria* immunized mice. The fixed bacteria coated on the beads were strictly identical to those used for the corresponding immunizations (same strain and batch).

Imaging and data analysis

The droplets in the 2D chamber were imaged using an inverted fluorescence microscope (Eclipse Ti2-E, Nikon) equipped with a motorized stage and excitation light (Lumencor Spectra X) at 37°C using a darkened cage incubator (Okolab). The images were recorded using a digital CMOS camera (ORCA-flash4.0 V2, Hamamatsu, in 2 × 2 binning mode) through a 10× objective (NA 0.45, Nikon). Large images composed of 10 × 10 fields of view (square size of 1.3 × 1.3 cm) were acquired, enabling to image of approximately 45,000 droplets. For the antibody secretion assay, images were recorded every 6 min for 30 min (six time points in total) in brightfield and DAPI, FITC, and Cy5 channels. For the bactoline assay, images were recorded every 8 min for 32 min (five time points in total) in brightfield and DAPI, FITC, TRITC, and Cy5 channels. The images were analyzed using DropMap, a custom MATLAB application described elsewhere [26, 27]. The total number of screened cells in each experiment was calculated by multiplying the total number of droplets by the λ (cells/droplets), counted using a custom MATLAB script as described before [55].

Antibody-SCs and C1q recruitment (for the bactoline assay only) were detected by an increase in fluorescence relocation of the corresponding detection probe: anti-mouse IgG Fc Alexa Fluor 647 (Cy5) for IgG, Zenon Alexa Fluor 488 mouse IgG1 labeling kit (FITC), AffiniPure F(ab')₂ Fragment Anti-Mouse IgM, μ chain specific, DyLight 405 labeled (DAPI) or Alexa Fluor 555-labeled C1q (TRITC). For each analyte (IgG, IgG1, IgM, or C1q), the corresponding limit of detection (LoD) was computed for each experi-

ment, adapted from a usual definition of the LoD [56], for example for IgG:

$$\text{LoD}_{\text{IgG}} = \text{median}_{\text{IgG empty droplets}} + 1.645 \times 2 \times k \times \text{MAD}_{\text{IgG empty droplets}}$$

where $\text{median}_{\text{IgG empty droplets}}$ is the median IgG probe relocation signal in empty droplets (without cells and thus without antibody secretion), $\text{MAD}_{\text{IgG empty droplets}}$ is the median absolute deviation of the IgG probe relocation signal in empty droplets, $k = 1.4826$ and $k \times \text{MAD}$ is a consistent estimator of the standard deviation σ , considering the distribution of relocation signals for empty droplets as normal. Droplets containing IgM- or IgG-SCs are then sorted based on the following criteria on the fluorescence relocation on the beadline of their corresponding detection probe: relocation above the LoD in at least one time point, relocation increasing over the time series, and relocation varying more over the time series than the analytical noise in the absence of antibody (defined as $\max_{\text{relocation}} - \min_{\text{relocation}} > 1.645 \times 2 \times k \times \text{MAD}_{\text{relocation in empty droplets}}$). The droplets that fulfill all three criteria are then visually verified using the DropMap MATLAB application to check for the absence of anomalies (fluorescent particle, clump of multiple cells, or other anomalies). Droplets containing IgG-SCs are further classified as IgG1 or IgG2a/2b/3 following the gating strategy displayed in Fig. 1C and Supporting Information Fig. S1B (horizontal gate is the LoD of IgG1).

Data representation and statistical analysis

In the different bar charts, each dot represents one mouse, and the mean and standard deviation are plotted for each condition. We used Welch's *t*-test to compute *p*-values. For the different scatter plots representing C1q against IgG or IgM binding densities (Fig. 3 and 4), each dot represents an antibody-secreting cell. To structure the data, we normalized the antibody relocation to its limit of detection (i.e. a value of 1 refers to a relocation = LoD), and we set an arbitrary limit between low- and high-density antibody binding considering all data sets (either IgG or IgM). This threshold corresponded, in an order of magnitude, to roughly 4 nM of relocated IgG in our calibration experiments with *P. aeruginosa*. We also used a limit between C1q binding and nonbinding antibodies that corresponded to the LoD of C1q binding. The C1q binding value displayed on the graphs was normalized by this LoD.

Acknowledgements: The European Research Council starting grant (grant #803'363), the Swiss National Science Foundation (grant #310030_197619), and the Branco Weiss – Society in Science Foundation supported this work. This work has benefited from the technical contribution of the joint service unit CNRS UAR

3750. The authors also thank Guilhem Chenon for the development of the DropMap application used for image analysis.

Conflict of interest: K.E. and J.B. hold several patents and are scientific co-founders of Saber Bio SAS, a company developing equipment for antibody discovery. The remaining authors declare no financial or commercial conflict of interest.

Author contributions: Nathan Aymerich planned, performed, and analyzed the experiments and drafted the manuscript. Luca J. Schlottheuber, Olivia T. M. Bucheli, and Kevin Portmann contributed to the mouse measurements. Klaus Eyer and Jean Baudry supervised the project. All authors commented on and revised the manuscript.

Ethics approval for animal studies: All procedures and immunizations were approved by the Cantonal ethics committee of Zürich described in this study under license number ZH215/19.

Data availability statement: The data that support the findings of this study are available from the corresponding author upon reasonable request.

Peer review: The peer review history for this article is available at <https://publons.com/publon/10.1002/eji.202451228>.

References

- Lapadula, G., Marchesoni, A., Armuzzi, A., Blandizzi, C., Caporali, R., Chimenti, S., Cimaz, R. et al., Adalimumab in the treatment of immune-mediated diseases. *Int. J. Immunopathol. Pharmacol.* 2014. 27: 33–48.
- Du, F. H., Mills, E. A. and Mao-Draayer, Y., Next-generation anti-CD20 monoclonal antibodies in autoimmune disease treatment. *Autoimmun. Highlights* 2017. 8: 12.
- Pierpont, T. M., Limper, C. B. and Richards, K. L., Past, present, and future of Rituximab-The world's first oncology monoclonal antibody therapy. *Front. Oncol.* 2018. 8:163.
- Kupferschmidt, K., Successful Ebola treatments promise to tame outbreak. *Science* 2019. 365: 628–629.
- Antimicrobial Resistance Collaborators, Global burden of bacterial antimicrobial resistance in 2019: a systematic analysis. *Lancet* 2022. 399: 629–655.
- Simonis, A., Kreer, C., Albus, A., Rox, K., Yuan, B., Holzmann, D., Wilms, J. et al., Discovery of highly neutralizing human antibodies targeting *Pseudomonas aeruginosa*. *Cell* 2023. 186: 5098–5113.e19.
- Attridge, S. R., Qadri, F., Albert, M. J. and Manning, P. A., Susceptibility of *Vibrio cholerae* O139 to antibody-dependent, complement-mediated bacteriolysis. *Clin. Diagn. Lab. Immunol.* 2000. 7: 444–450.
- Hellerud, B. C., Aase, A., Herstad, T. K., Næss, L. M., Kristiansen, L. H., Trøseid, A. M. S., Harboe, M. et al., Critical roles of complement and antibodies in host defense mechanisms against *Neisseria meningitidis* as revealed by human complement genetic deficiencies. *Infect. Immun.* 2010. 78: 802–809.
- Geurtsen, J., Fae, K. C. and Dobbelssteen, G., Importance of (antibody-dependent) complement-mediated serum killing in protection against *Bordetella pertussis*. *Expert Rev. Vaccines* 2014. 13: 1229–1240.
- Gulati, S., Beurskens, F. J., de Kreuk, B. J., Roza, M., Zheng, B., Deoliveira, R. B., Shaughnessy, J. et al., Complement alone drives efficacy of a chimeric antigonococcal monoclonal antibody. *PLoS Biol.* 2019. 17: e3000323.
- Gil, E., Noursadeghi, M. and Brown, J. S., Streptococcus pneumoniae interactions with the complement system. *Front. Cell. Infect. Microbiol.* 2022. 12: 929483.
- Ricklin, D., Hajishengallis, G., Yang, K. and Lambris, J. D., Complement: a key system for immune surveillance and homeostasis. *Nat. Immunol.* 2010. 11: 785–797.
- Gaboriaud, C., Thielens, N. M., Gregory, L. A., Rossi, V., Fontecilla-Camps, J. C. and Arlaud, G. J., Structure and activation of the C1 complex of complement: unraveling the puzzle. *Trends Immunol.* 2004. 25: 368–373.
- Haas, P. J. and Strijp, J. V., Anaphylatoxins: their role in bacterial infection and inflammation. *Immunol. Res.* 2007. 37: 161–175.
- Klos, A., Tenner, A. J., Johswich, K. O., Ager, R. R., Reis, E. S. and Köhl, J., The role of the anaphylatoxins in health and disease. *Mol. Immunol.* 2009. 46: 2753–2766.
- Dunkelberger, J. R. and Song, W. C., Complement and its role in innate and adaptive immune responses. *Cell Res.* 2010. 20: 34–50.
- Krych-Goldberg, M. and Atkinson, J. P., Structure-function relationships of complement receptor type 1. *Immunol. Rev.* 2001. 180: 112–122.
- van Lookeren Campagne, M., Wiesmann, C. and Brown, E. J., Macrophage complement receptors and pathogen clearance. *Cell. Microbiol.* 2007. 9: 2095–2102.
- Tegla, C. A., Cudrici, C., Patel, S., Trippe, R., Rus, V., Niculescu, F. and Rus, H., Membrane attack by complement: the assembly and biology of terminal complement complexes. *Immunol. Res.* 2011. 51 45–60.
- Collins, M., IgG subclass co-expression brings harmony to the quartet model of murine IgG function. *Immunol. Cell Biol.* 2016. 94: 949–954.
- Michaelsen, M., Garred, P. and Aase, A., Human IgG subclass pattern of inducing complement-mediated cytotoxicity depends on antigen concentration and to a lesser extent on epitope patchiness, antibody affinity and complement concentration. *Eur. J. Immunol.* 1991. 21: 11–16.
- Diebolder, A., Beurskens, F. J., Jong, R. N. D., Koning, R. I., Strumane, K., Lindorfer, M. A., Voorhorst, M. et al., Complement is activated by IgG hexamers assembled at the cell surface. *Science* 2014. 343: 1260–1263.
- Wang, G., de Jong, R. N., van den Bremer, E. T. J., Beurskens, F. J., Labrijn, A. F., Ugurlar, D., Gros, P. et al., Molecular basis of assembly and activation of complement component C1 in complex with immunoglobulin G1 and antigen. *Mol. Cell* 2016. 63: 135–145.
- Ugurlar, D., Howes, S. C., Kreuk, B. J. D., Koning, R. I., Jong, R. N. D., Beurskens, F. J., Schuurman, J. et al., Structures of C1-IgG1 provide insights into how danger pattern recognition activates complement. *Science* 2018. 359: 794–797.
- Sharp, T. H., Boyle, A. L., Diebolder, C. A., Kros, A., Koster, A. J. and Gros, P., Insights into IgM-mediated complement activation based on in situ structures of IgM-C1-C4b. *Proc. Nat. Acad. Sci. USA* 2019. 116: 11900–11905.
- Eyer, K., Doineau, R. C. L., Castrillon, C. E., Briseno-Roa, L., Menrath, V., Mottet, G., England, P. et al., Single-cell deep phenotyping of IgG-secreting cells for high-resolution immune monitoring. *Nat. Biotechnol.* 2017. 35: 977–982.
- Bounab, Y., Eyer, K., Dixneuf, S., Rybczynska, M., Chauvel, C., Mistretta, M., Tran, T. et al., Dynamic single-cell phenotyping of immune cells using the microfluidic platform DropMap. *Nat. Protoc.* 2020. 15: 2920–2955.
- Taly, V., Descroix, S. and Perez-Toralla, K. (eds.), A guide to the quantitation of protein secretion dynamics at the single-cell level. *Microfluidics diagnostics: methods and protocols*. Methods in Molecular Biology. Vol. 2804, Humana New York, NY, 2024.

- 29 Nossal, G. J. and Lederberg, J., Antibody production by single cells. *Nature* 1958. **181**: 1419–1420.
- 30 Heo, M., Chenon, G., Castrillon, C., Bibette, J., Bruhns, P., Griffiths, A. D., Baudry, J. et al., Deep phenotypic characterization of immunization-induced antibacterial IgG repertoires in mice using a single-antibody bioassay. *Commun. Biol.* 2020. **3**: 614.
- 31 Zwarthoff, S. A., Widmer, K., Kuipers, A., Strasser, J., Ruyken, M., Aerts, P. C., de Haas, C. J. C. et al., C1q binding to surface-bound IgG is stabilized by C1r2s2 proteases. *Proc. Nat. Acad. Sci. USA* 2021. **118**: e2102787118.
- 32 Damelang, T., de Taeye, S. W., Rentenaar, R., Roya-Kouchaki, K., de Boer, E., Derksen, N. I. L., van Kessel, K. et al., The influence of human IgG subclass and allotype on complement activation. *J. Immunol.* 2023. **211**: 1725–1735.
- 33 Oskam, N., Ooijevaar-de Heer, P., Derksen, N. I. L., Kruihof, S., de Taeye, S. W., Vidarsson, G., Reijm, S. et al., At critically low antigen densities, IgM hexamers outcompete both IgM pentamers and IgG1 for human complement deposition and complement-dependent cytotoxicity. *J. Immunol.* 2022. **209**: 16–25.
- 34 Strasser, J., de Jong, R. N., Beurskens, F. J., Wang, G., Heck, A. J. R., Schuurman, J., Parren, P. et al., Unraveling the macromolecular pathways of IgG oligomerization and complement activation on antigenic surfaces. *Nano Lett.* 2019. **19**: 4787–4796.
- 35 Silveira, S. A. D., Kikuchi, S., Fossati-Jimack, L., Moll, T., Saito, T., Verbeek, J. S., Botto, M. et al., Complement activation selectively potentiates the pathogenicity of the IgG2b and IgG3 isotypes of a high affinity anti-erythrocyte autoantibody. *J. Exp. Med.* 2002. **195**: 665–672.
- 36 Lilienthal, G. M., Rahmüller, J., Petry, J., Bartsch, Y. C., Leliavski, A. and Ehlers, M., Potential of murine IgG1 and Human IgG4 to inhibit the classical complement and Fcγ receptor activation pathways. *Front. Immunol.* 2018. **9**: 1.
- 37 Michaelsen, T. E., Kolberg, J., Aase, A., Herstad, T. K. and Høiby, E. A., The four mouse IgG isotypes differ extensively in bactericidal and opsonophagocytic activity when reacting with the P1.16 epitope on the outer membrane PorA protein of *Neisseria meningitidis*. *Scand. J. Immunol.* 2004. **59**: 34–39.
- 38 Neuberger, M. S. and Rajewsky, K., Activation of mouse complement by monoclonal mouse antibodies. *Eur. J. Immunol.* 1981. **11**: 1012–1016.
- 39 Giuntini, S., Reason, D. C. and Granoff, D. M., Combined roles of human IgG subclass, alternative complement pathway activation, and epitope density in the bactericidal activity of antibodies to meningococcal factor H binding protein. *Infect. Immun.* 2012. **80**: 187–194.
- 40 Wright, J. K., Tschopp, J., Jaton, J. C. and Engel, J., Dimeric, trimeric and tetrameric complexes of immunoglobulin G fix complement. *Biochem. J.* 1980. **187**: 775–780.
- 41 Mortensen, S. A., Sander, B., Jensen, R. K., Pedersen, J. S., Golas, M. M., Jensenius, J. C., Hansen, A. G. et al., Structure and activation of C1, the complex initiating the classical pathway of the complement cascade. *Proc. Nat. Acad. Sci. USA* 2017. **114**: 986–991.
- 42 Abendstein, L., Noteborn, W. E. M., Veenman, L. S., Dijkstra, D. J., van de Bovenkamp, F. S., Trouw, L. A. and Sharp, T. H., DNA nanostructure-templated antibody complexes provide insights into the geometric requirements of human complement cascade activation. *J. Am. Chem. Soc.* 2024. **146**: 13455–13466.
- 43 Bindon, C. I., Hale, G. and Waldmann, H., Importance of antigen specificity for complement-mediated lysis by monoclonal antibodies. *Eur. J. Immunol.* 1988. **18**: 1507–1514.
- 44 Cragg, M. S., Morgan, S. M., Chan, H. T. C., Morgan, B. P., Filatov, A. V., Johnson, P. W. M., French, R. R. et al., Complement-mediated lysis by anti-CD20 mAb correlates with segregation into lipid rafts. *Blood* 2003. **101**: 1045–1052.
- 45 Teeling, J. L., Mackus, W. J. M., Wiegman, L., van den Brakel, J. H. N., Beers, S. A., French, R. R., van Meerten, T. et al., The biological activity of human CD20 monoclonal antibodies is linked to unique epitopes on CD20. *J. Immunol.* 2006. **177**: 362–371.
- 46 Teeling, J. L., French, R. R., Cragg, M. S., Brakel, J. V. D., Pluyter, M., Huang, H., Chan, C. et al., Characterization of new human CD20 monoclonal antibodies with potent cytolytic activity against non-Hodgkin lymphomas. *Blood* 2004. **104**: 1793–1800.
- 47 Pawluczko, W., Beurskens, F. J., Beum, P. V., Lindorfer, M. A., van de Winkel, J. G. J., Parren, P. and Taylor, R. P., Binding of submaximal C1q promotes complement-dependent cytotoxicity (CDC) of B cells opsonized with anti-CD20 mAbs Ofatumumab (OFA) or Rituximab (RTX): considerably higher levels of CDC are induced by OFA than by RTX. *J. Immunol.* 2009. **183**: 749–758.
- 48 Cleary, K. L. S., Chan, H. T. C., James, S., Glennie, M. J. and Cragg, M. S., Antibody distance from the cell membrane regulates antibody effector mechanisms. *J. Immunol.* 2017. **198**: 3999–4011.
- 49 Xia, M.-Q., Hale, G. and Waldmann, H., Efficient complement-mediated lysis of cells containing the CAMPATH-1 (CDw52) antigen. *Mol. Immunol.* 1993. **30**: 1089–1096.
- 50 Perkins, S. J., Nealis, A. S., Sutton, B. J. and Feinstein, A., Solution structure of human and mouse immunoglobulin M by synchrotron X-ray scattering and molecular graphics modelling. A possible mechanism for complement activation. *J. Mol. Biol.* 1991. **221**: 1345–1366.
- 51 Müller, R., Gräwert, M. A., Kern, T., Madl, T., Peschek, J., Sattler, M., Groll, M. et al., High-resolution structures of the IgM Fc domains reveal principles of its hexamer formation. *Proc. Nat. Acad. Sci. USA* 2013. **110**: 10183–10188.
- 52 Czajkowsky, D. M. and Shao, Z., The human IgM pentamer is a mushroom-shaped molecule with a flexural bias. *Proc. Nat. Acad. Sci. USA* 2009. **106**: 14960–14965.
- 53 Chen, Q., Menon, R., Calder, L. J., Tolar, P. and Rosenthal, P. B., Cryomicroscopy reveals the structural basis for a flexible hinge motion in the immunoglobulin M pentamer. *Nat. Commun.* 2022. **13**.
- 54 Son, M., Understanding the contextual functions of C1q and LAIR-1 and their applications. *Exp. Mol. Med.* 2022. **54**: 567–572.
- 55 Portmann, K., Linder, A., Oelgarth, N. and Eyer, K., Single-cell deep phenotyping of cytokine release unmasks stimulation-specific biological signatures and distinct secretion dynamics. *Cell Rep. Methods* 2023. **2**: 100502.
- 56 Armbruster, D. A. and Pry, T., Limit of blank, limit of detection and limit of quantitation. *Clin. Biochem. Rev.* 2008. **29**: 49–52.

Abbreviations: SC: secreting cell · LoD: limit of detection

Full correspondence: Dr. Jean Baudry, Laboratoire Colloïdes et Matériaux Divisés (LCMD), ESPCI Paris, PSL Research University, CNRS UMR8231 Chimie Biologie Innovation, 75005 Paris, France
e-mail: jean.baudry@espci.fr
Dr. Klaus Eyer, Department of Biomedicine, Aarhus University, 8000 Aarhus C, Denmark
e-mail: eyerk@biomed.au.dk

Received: 30/4/2024

Revised: 23/8/2024

Accepted: 24/8/2024

Accepted article online: 26/5/2024